Advancing FIB assisted 3D EBSD using a static sample setup

Julien Guyon, Nathalie Gey, Daniel Goran, Smail Chalal, Fabian Perez-Willard

Advancing FIB assisted 3D EBSD using a static sample setup

Julien Guyon [a,b], Nathalie Gey [a,b,*], Daniel Goran [c], Smail Chalal [d], Fabián Pérez-Willard [d]

[a] Laboratoire d'Etude des Microstructures et de Mécanique des Matériaux, LEM3, CNRS ISGMP, Université de Lorraine, F-57045 Metz Cedex 01, France
[b] Laboratory of Excellence on Design of Alloy Metals for low-mAss Structures ('LabEx DAMAS'), Université de Lorraine, F-57045 Metz Cedex 01, France
[c] Bruker Nano GmbH, Am Studio 2D, 12489 Berlin, Germany
[d] Carl Zeiss Microscopy GmbH, Carl-Zeiss Street 56, 73447 Oberkochen, Germany

ARTICLE INFO

Keywords:
FIB–SEM
3D EBSD
Static setup
Tomography
Grain boundary

ABSTRACT

A new setup for automatic 3D EBSD data collection in static mode has been developed using a conventional FIB–SEM system. This setup requires no stage or sample movements between the FIB milling and EBSD mapping. Its capabilities were tested experimentally on a coherent twin boundary of an INCONEL sample. Our result demonstrates that this static setup holds many advantages in terms of data throughput and quality as compared with other ones requiring stage/sample movements. The most important advantages are the better slice alignment and an improved orientation precision in 3D space, both being prerequisite for a reliable grain boundary characterization.

1. Introduction

Electron backscatter diffraction (EBSD) is an experimental technique, which is used to study the crystallographic microstructure of polycrystalline specimens in the SEM [1]. Applications of EBSD in the fields of materials science, especially metallography, and geological sciences are manifold.

EBSD allows determination of crystal structure and orientation of the different grains present in the sample. Typically, EBSD maps are acquired by scanning point by point a flat polished sample surface with the SEM beam while collecting EBSD patterns simultaneously.

Recently, the need for a comprehensive characterization of grains and grain boundaries has led to the extension of EBSD into three dimensions (3D). 3D EBSD can be performed by serial sectioning the sample with robot assisted grinding and polishing [2], laser ablation [3], or focused ion beam (FIB) milling [4] in an automated process. The result is a stack of 2D EBSD maps, which can be rendered to a 3D volume.

In this note we report about an optimized experimental setup for 3D EBSD data acquisition in a conventional FIB–SEM instrument. In contrast to other 3D EBSD experiments, in our setup the sample remains static during the entire experiment. The advantages in terms of data quality and throughput are discussed and illustrated with 3D EBSD measurements on a coarse-grained INCONEL 718 nickel-based superalloy sample containing coherent annealing twins.

* Corresponding author at: Laboratoire d'Etude des Microstructures et de Mécanique des Matériaux, LEM3, CNRS ISGMP, Université de Lorraine, F-57045 Metz Cedex 01, France.
E-mail address: nathalie.gey@univ-lorraine.fr (N. Gey).

2. Different 3d EBSD setups

During 3D EBSD in the FIB–SEM instrument thin slices of sample material are removed by FIB and the exposed surfaces analyzed with EBSD. FIB milling and EBSD mapping are repeated sequentially, usually hundreds of times, to analyze the total volume of interest.

Often, this is achieved by moving the sample back and forth between a FIB milling and an EBSD position. In the FIB position, the FIB beam is in grazing incidence with the surface prepared for EBSD – surface normal $\vec{N}$. In the EBSD position, $\vec{N}$ is at an angle of 70° to the SEM beam direction $\vec{E}$, and the EBSD camera axis lies in the plane spanned by $\vec{N}$ and $\vec{E}$.

2.1. Rotation and tilt setup

Depending on the location of the EBSD camera relative to the FIB column, different stage movements will be needed between milling and EBSD positions. Following the nomenclature in Ref. [4] rotation and tilt setup can be distinguished.

Fig. 1(a) illustrates the rotation setup. EBSD camera and FIB are on the same side of the microscope chamber. Interchange of EBSD and milling positions involves mainly a stage rotation movement (besides *X*, *Y*, and *Z* movements).

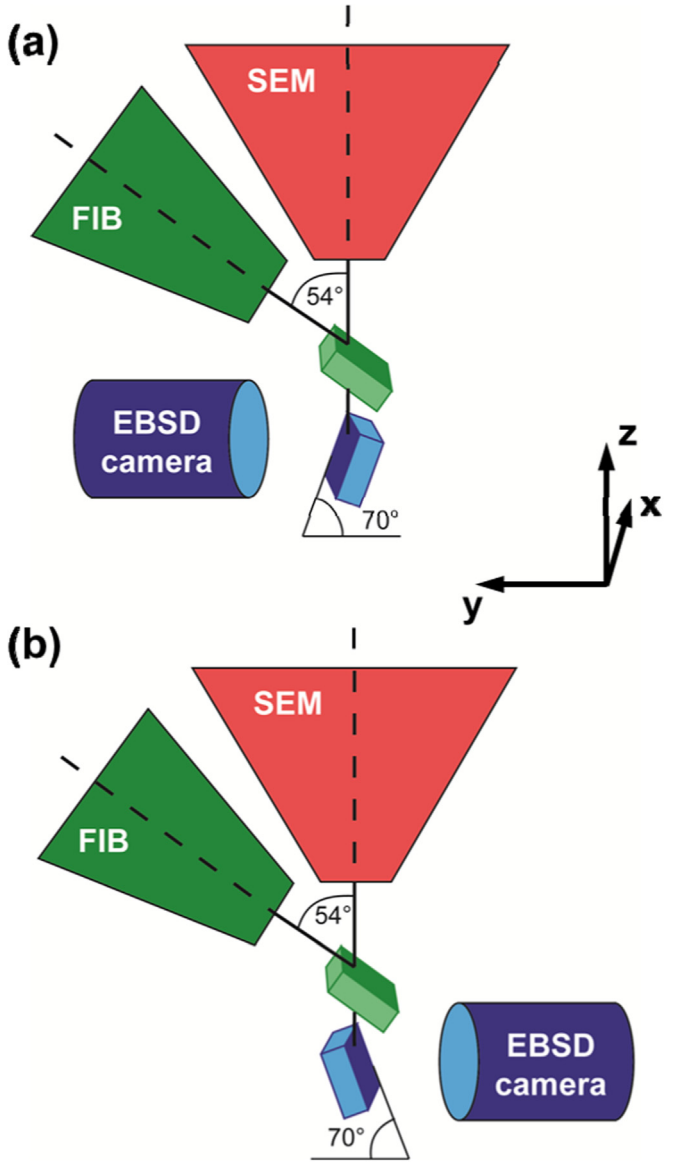

Fig. 1. Schematic drawing of the (a) rotation and (b) tilt setup. The green and blue rectangular prisms show the sample in milling and EBSD position, respectively.

Fig. 1(b) shows the tilt setup. Here, EBSD and FIB are on opposite sides of the chamber. Movements between milling and EBSD positions require a change in specimen tilt.

Commercially available 3D EBSD FIB–SEM solutions are commonly based on the rotation geometry [5]. The tilt setup has been realized in [6].

After every stage movement, image recognition is used to ensure accurate positioning of FIB and SEM beams relative to the region of interest. SEM and FIB beam shift corrections are applied along *X* and *Y* image directions.

Moreover, additional angular misalignment of the sample and inaccuracy in *Z* sample position after the rotation or tilt movement are also observed. If not corrected for, these result in distortions and defocus of the SEM image. Furthermore, the thickness uniformity of the milled slices is compromised. For the EBSD measurement, indexing rate and 3D angular resolution are degraded. In summary, 3D crystallographic interface analysis becomes rather inaccurate.

Obviously, the most powerful setup to overcome the aforementioned drawbacks would be a 'static setup' with no sample movement between milling and EBSD measurement. Recently, an static approach has been reported using a FIB–SEM system with an orthogonal arrangement of FIB and SEM [7]. In this note we report a static configuration on a conventional FIB–SEM.

2.2. The static 3D EBSD setup

In the so called static EBSD geometry, FIB material removal and EBSD analysis are done at the coincidence point of FIB and SEM beams without any stage movements. The following two conditions need to be fulfilled:

First, the normal $\vec{N}$ of the prepared surface is at 70° tilt to the SEM beam $\vec{E}$ (standard EBSD condition), i.e.

$$\angle\left(\vec{E},\ \vec{N}\right) = 70^\circ \tag{1}$$

Second, the FIB beam direction $\vec{I}$ is parallel to the FIB prepared surface (grazing incidence condition), i.e.

$$\vec{I}\cdot\vec{N} = 0 \tag{2}$$

Eqs. (1) and (2) can be solved easiest using spherical coordinates $(r,\ \theta,\ \varphi)$. For the following the coordinate system has been defined as shown in Figs. 1 and 2.

The EBSD condition, Eq. (1), is illustrated in Fig. 2(a). It forces the vector $\vec{N}$ (blue arrow) to lie on the surface of a cone with an opening half-angle of 70° around $\vec{E}$. This results in the polar angle $\theta = 70^\circ$ for $\vec{N}$. The FIB grazing incidence condition, Eq. (2), forces $\vec{N}$ to lie in the plane perpendicular to $\vec{I}$, which is blue shaded in Fig. 2 (b). The combination of both conditions yields two solutions for $\vec{N}$ corresponding to the two intersections lines of the blue plane (Fig. 2(b)) with the cone (Fig. 2(a)). These two solutions for $\vec{N}$ are defined by the azimuthal angles φ_1 and $\varphi_2 = 180^\circ - \varphi_1$. Fig. 2 (c) shows φ_1 solution whereas Fig. 2(d) shows the two solutions projected into the xy plane. φ_1 and φ_2 depend only on the angle θ_{FIB} between FIB and SEM columns [8]. Thus, the possible orientations of $\vec{N}$ are fully defined, which in turn determine the ideal positions of the EBSD camera.

In the next section the realization of such a static setup for 3D EBSD in a conventional FIB–SEM instrument is described.

3. Experimental setup and methods

3.1. Implementation of static 3D EBSD

In this work, the static 3D EBSD setup is realized on a customized ZEISS Auriga 40 FIB–SEM instrument. The FIB–SEM coincidence point of this instrument is at a working distance (WD) of 5 mm. Given the angle of 54° between FIB and SEM columns θ_{FIB}=54°, the azimuthal angle that defines the sample position for static EBSD is $\varphi_1 = -15.3^\circ$ and $\varphi_2 = 180^\circ + 15.3^\circ$.

The original chamber of the ZEISS Auriga 40 was redesigned to accommodate the EBSD camera at $\varphi = \varphi_1 = -15.3^\circ$ with the camera facing the sample and fulfilling the standard EBSD condition (see Fig. 3 and text above).

To guarantee beam stability and reduced drifts during long experiments, the microscope is operated remotely and housed in a room with optimized acoustic, electromagnetic and thermal (< 0.5 °C/h) conditions.

The FIB–SEM is equipped with a high resolution Bruker e-Flash EBSD detector. The geometry of the detector allows its insertion up to a distance of 15 mm to the coincidence point at WD = 5 mm. Both, image resolution and in-lens detection efficiency benefit from the short WD.

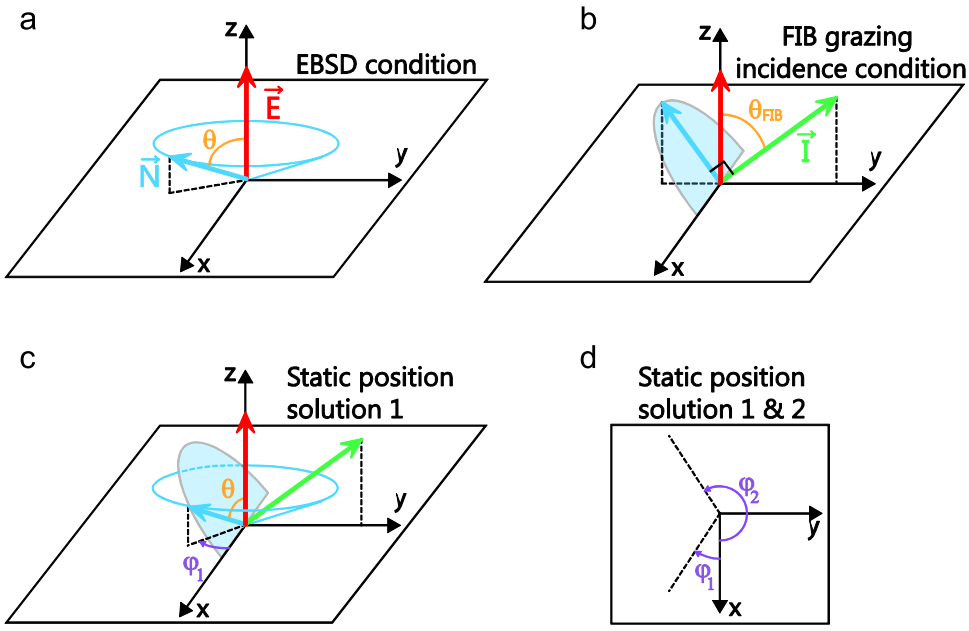

Fig. 2. Illustration of the static 3D EBSD setup geometry. Both, standard EBSD (a) and FIB grazing incidence (b) conditions need to be fulfilled by the FIB prepared surface normal $\vec{N}$. (c) shows one of two possible solutions and (d) the projection of the two solutions into the *xy* plane with their azimuthal angles φ_1 and φ_2. (For interpretation of the references to color in this figure, the reader is referred to the web version of this article.)

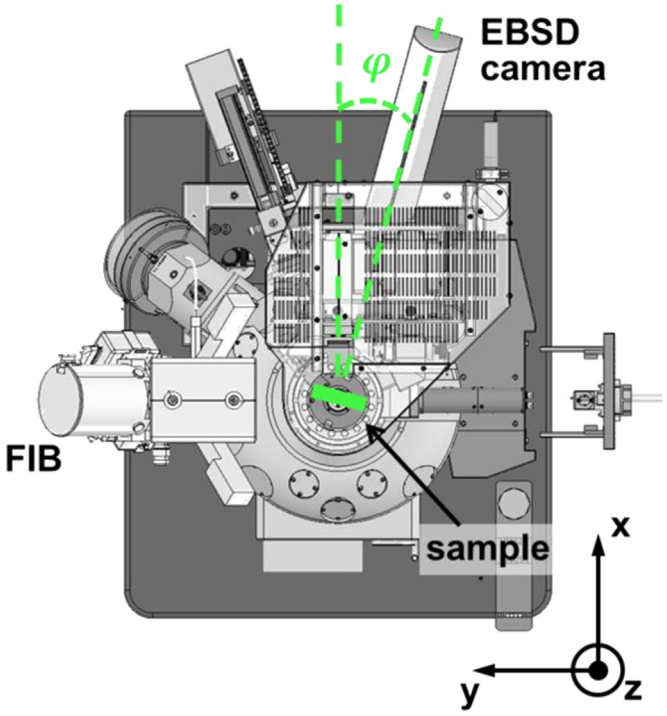

Fig. 3. Top view CAD drawing of the customized ZEISS Auriga. The azimuthal angle for the EBSD camera $\varphi = -15.3°$.

3.2. D EBSD data acquisition

The 3D EBSD acquisition workflow has been fully automated. For this purpose, a homemade software with a new user interface (UI) was developed at LEM3 using the Application Programming Interfaces (API) of ZEISS FIB–SEM and Bruker EBSD systems. This acquisition software triggers all milling, image and EBSD acquisition processes. All FIB–SEM operations can be set directly within the UI. EBSD acquisition parameters are defined in the EBSD software as for a usual 2D EBSD map. From one slice to the next, the EBSD map area is tracked by applying constant SEM beam shifts and focus corrections. These compensate for

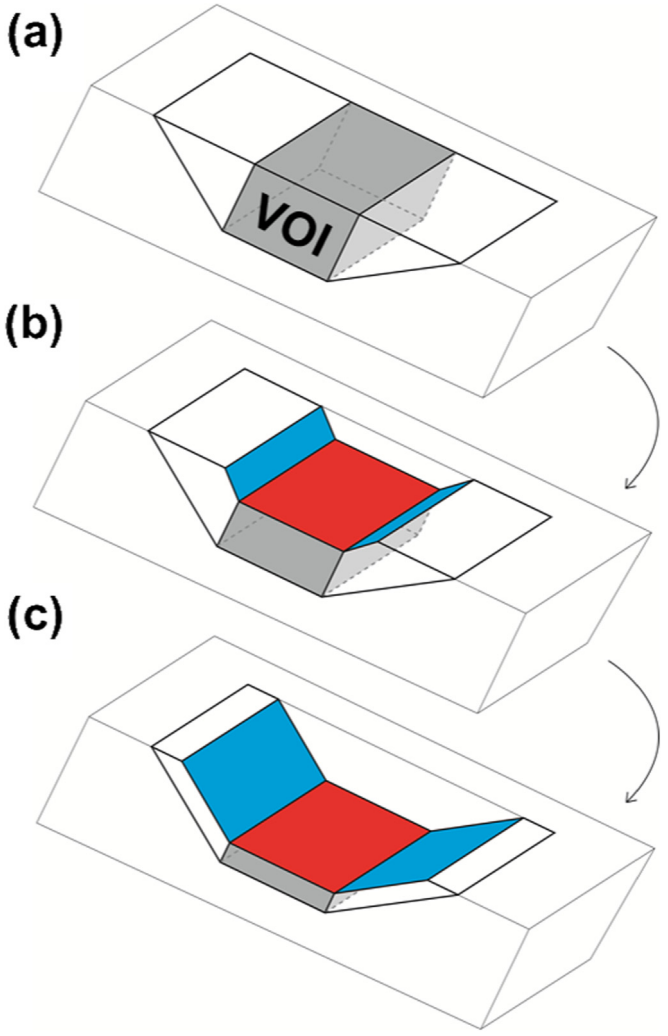

Fig. 4. Schematic showing the sample from the SEM perspective before 3D EBSD acquisition (a), and towards the beginning (b) and end (c) of the experiment. The volume of interest is shaded in gray color.

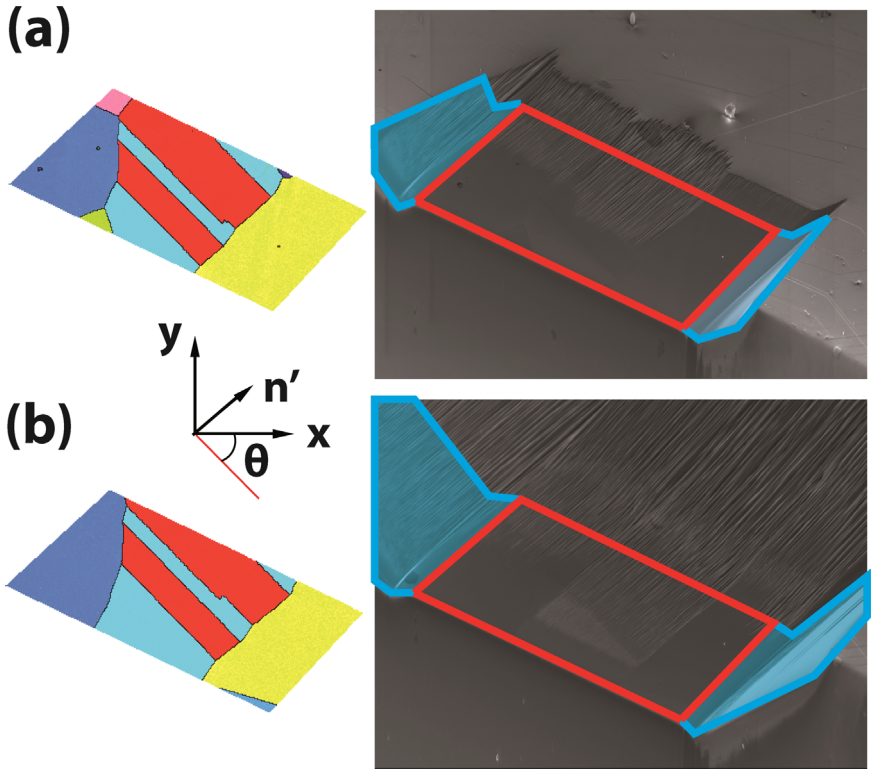

Fig. 5. EBSD map and SEM image of the INCONEL 718 sample after FIB milling of slices 20 (a) and 67 (b). The red frame in the SEM images shows the area from which EBSD data was collected. The twins of the central grain intercept the (x,y) plane with an angle θ relative to the x-axis (see inset). $\vec{n}'$ is the normal to the twin traces. (For interpretation of the references to color in this figure legend, the reader is referred to the web version of this article.)

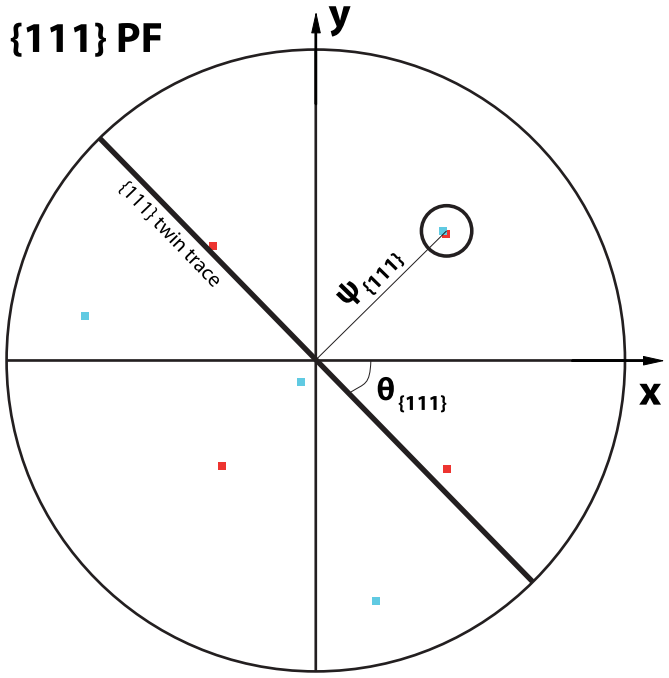

Fig. 6. {111} Pole figure of the targeted grain and twin orientations. The color code is the same as in Fig. 5. The {111} twin pole (common to both orientations) is encircled. The angles (θ=45°, ψ=60.6°) define the position of the coherent twin plane in the (x,y,z) sample coordinate system (its trace in the (x,y) projection plane is indicated by the black line).

the removed targeted slice thickness. Additional image recognition to correct for image drift is considered optional in the static setup.

During the 3D EBSD run, acquired 2D EBSD data and SEM images can be visualized at any time in the UI.

3.3. Experiment

A nickel-based superalloy INCONEL 718 sample was used as a model material to test our experimental setup. Nickel is well suited for this study because it yields high-quality EBSD patterns on 30 kV FIB polished surfaces even at high EBSD acquisition speeds (in this experiment, 140 Hz, i.e. 7 ms per pattern). Moreover, the Ni grains contain numerous coherent twins. These are characterized by well-known {111} boundary planes, which are used as a reference to evaluate raw data alignment.

The sample was roughly $(10 \times 10 \times 5)\,\mathrm{mm}^3$ in size. Two adjacent faces of the sample were polished carefully to form an orthogonal angle.

For the 3D EBSD measurement, the sample was mounted on a 70° pre-tilted holder. Accessible volumes of interest are located in the sample edge between its two polished faces. For convenience, the sample was oriented on the holder such that this edge is on the top and is perpendicular to the FIB beam once the final static position has been reached. After loading the sample into the FIB–SEM, the microscope stage was rotated in order to orient the face dedicated to further EBSD analysis towards the camera. Finally, the volume of interest is positioned at the FIB–SEM coincidence point. The sample will remain in this position until the complete 3D EBSD run is finished.

Before the 3D EBSD was started, an approximately 1 μm-thick protective layer of carbon was deposited on top of the volume of interest (VOI) by electron and FIB induced deposition.

Fig. 4 shows the sample schematically at three different stages of the static 3D EBSD run. The top image (a) shows the sample before the 3D EBSD acquisition has started. The VOI is shaded in gray color. (b) and (c) show the sample towards the beginning and end of the run, respectively. The red surfaces show the FIB polished area from which EBSD data is acquired. Before a new slice is removed, excavations left and right of the slice are done. The blue

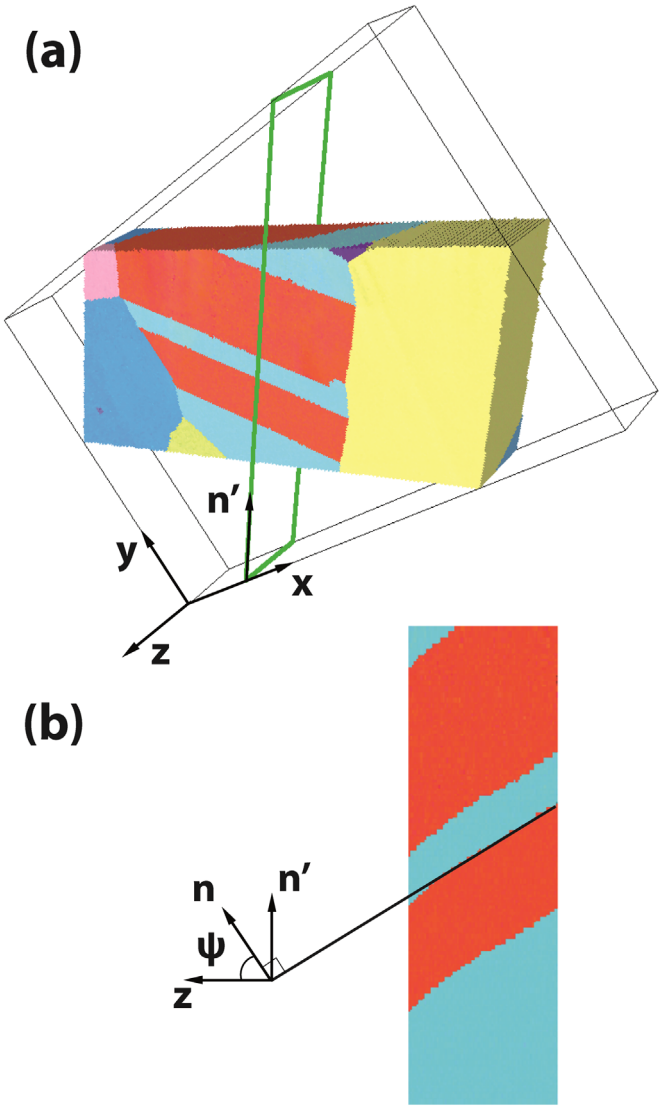

Fig. 7. (a) Reconstructed 3D EBSD volume from the perspective of the FIB polished surfaces. (b) Data volume sectioned along a plane (green frame in 6(a)) perpendicular to the EBSD acquisition plane and containing the normal $\vec{n}'$ to the twin traces. (For interpretation of the references to color in this figure legend, the reader is referred to the web version of this article.)

surfaces in (b) and (c) result from these side cuts. The side cuts prevent the trench edges from obstructing either the incident electron beam or the diffracted signal as the FIB works its way through the VOI. Sequential side cutting has the additional advantage that it removes redeposited material (generated during the previous slice cutting) which can also shadow the EBSD detector. The size of the side cuts increases with slice number. The Acquisition Software calculates their exact shape aiming to minimize milling time by targeting only material in the required angle of view. The side excavations of all slices add up to the two triangular prisms shown in (a) left and right of the VOI. For this experiment, side and main slice cuts were done (in this order) at 30 nA and 4 nA FIB currents, respectively.

In our experiment, 75 slices were measured in total. The targeted slice thickness was 200 nm. Thus, a VOI of $(100 \times 45 \times 15)\ \mu m^3$ was analyzed. The experiment took approx. 30 h. During the run, only calculated beam shift and focus corrections were applied (see above) and no image recognition was used.

For rendering and analysis of the 3D EBSD data the software packages referenced in [9] were used.

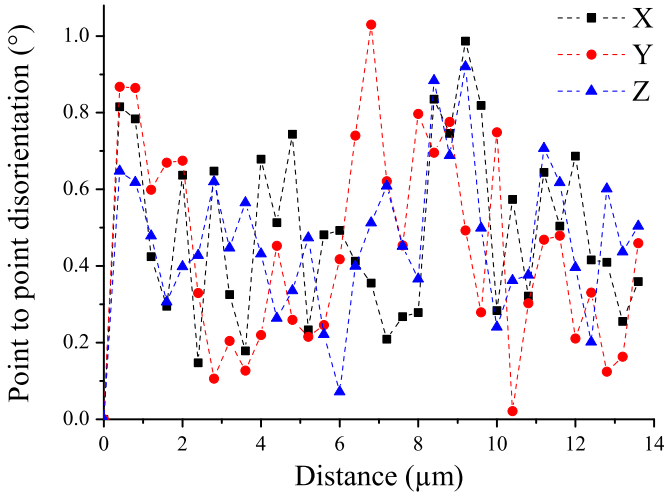

Fig. 8. Disorientation profile measured in the 3 directions *x*, *y*, and *z* within the red grain in the center of our VOI. (For interpretation of the references to color in this figure legend, the reader is referred to the web version of this article.)

4. Results

Fig. 5 shows two EBSD maps acquired on the INCONEL 718 sample corresponding to slices 20 (a) and 67 (b). Each EBSD map covers an area of $(100 \times 45)\ \mu m^2$ and was measured with a step size of 400 nm. The red frames on the SEM images (on the right hand side of Fig. 5) show the areas from which the EBSD maps were collected. The blue shaded faces are the result of the side cuts (cf. Fig. 4). In the following, crystallographic orientations are measured relative to the (*x*,*y*,*z*) sample coordinate system shown in the insets, where the *z*-axis points out of the figure.

The twinned grain (cyan and red colors) in the center of the EBSD maps was originally targeted as the VOI. The twin planes intersect the (*x*,*y*) plane in parallel traces. The traces form an angle θ with the *x*-axis (see inset). $\vec{n}'$ is the normal to these traces.

The twinned grain serves as a model system to evaluate how accurately grain boundaries can be reconstructed in 3D. Assuming a coherent twin, the boundary should be a {111} plane. The position of this {111} twin plane in the (*x*,*y*,*z*) coordinate system is fully determined by the grain and twin orientations.

Fig. 6 gives the stereographic projection of the {111} poles for the average orientations of the grain and the twin. These orientations were calculated from the EBSD map of slice 20; they are described by the set of three Euler angles as follows: $(\varphi_1, \varphi, \varphi_2)_{grain} = (22.3°, 48.6°, 34.7°)$ and $(\varphi_1, \varphi, \varphi_2)_{twin} = (293.3°, 6.1°, 68.0°)$. The {111} twin pole (common to both orientations) is encircled and the trace of the corresponding plane in the (*x*,*y*) projection plane is indicated by the black line. The grain orientation matrix was used to calculate the exact position of the {111} plane in the (*x*,*y*,*z*) sample coordinate system: it intersects the (*x*, *y*) projection plane in a line with an angle $\theta_{\{111\}}=45.0°$ relative to the *x*-axis and has an polar angle $\psi_{\{111\}} = 60.6°$ relative to the *z*-axis. These angles are indicated in Fig. 6. Notice that the theoretical position of the twin plane varies slightly within the precision of the orientation determination of $(\varphi_1, \varphi, \varphi_2)_{grain}$ and $(\varphi_1, \varphi, \varphi_2)_{twin}$. This theoretical position of the {111} twin plane will be compared in what follows with the experimental twin boundary plane position deduced from the 3D data set.

The 75 slices were piled up to render the 3D EBSD volume shown in Fig. 7. No data processing was performed to align the different slices to each other. The orientation color code is the same as in Fig. 5.

Fig. 7(a) shows an overview of the 3D EBSD volume. The volume was sectioned along the plane highlighted by the green frame and rotated towards the viewer (Fig. 7(b)). The sectioned

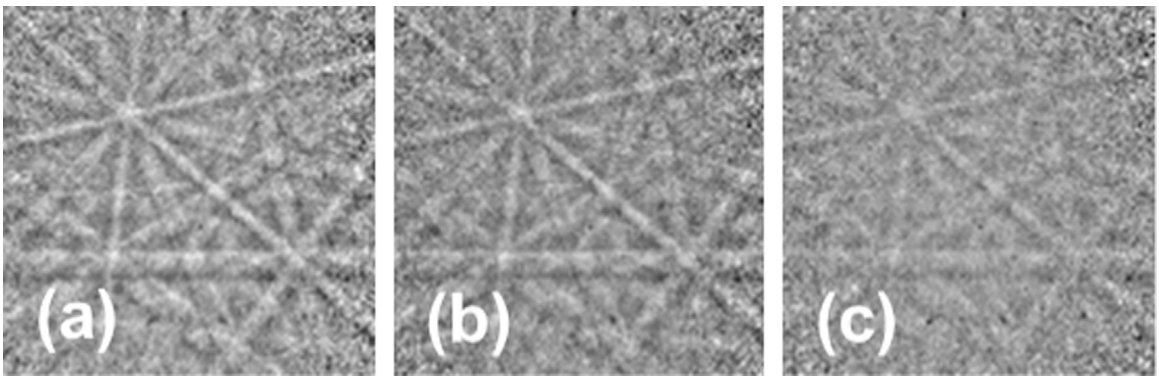

Fig. 9. EBSD patterns of the same grain. Patterns (b) and (c) were measured while polishing with a 4 nA and a 30 nA FIB beam, respectively. For comparison the pattern (a) was acquired without simultaneous milling on a 4 nA FIB polished surface.

plane is spanned by the normal $\vec{n}'$ of the twin trace in the (x,y) plane and the z-axis. The reconstructed twin boundaries appear almost perfectly flat as can be expected for twin boundaries. This proves a very good alignment of the raw (unprocessed) data. Only for the 10 first slices, the reconstructed boundary deviates slightly from a straight line. This is due to short-term thermal and electronic drift of the system at the beginning of the measurement.

A deeper analysis of the 3D data set confirms important advantages of the static setup, which are listed in the following:

(1) The static setup guarantees the same EBSD angular resolution across the slices as within each slice. No additional orientation spread is introduced in the same grain, from one slice to the next. Indeed, the angular disorientations between adjacent voxels of the same grain were found to be of the same order of magnitude for all 3 spatial directions x, y, and z. Fig. 8 gives an example of a disorientation profile measured along x, y, and z for the red grain in the center of our VOI. The point to point disorientations are similar in all 3 directions and mostly lower than 1° (as expected according to our EBSD data acquisition setting). This contrasts with results obtained with a non-static setup where the angular resolution along z will depend on the accuracy of the stage repositioning after movement between milling and EBSD data acquisition steps.
(2) Negligible image distortions were observed between the different slices. As seen for example in slices 20 and 67 of Fig. 5, the traces of the targeted twin plane are well aligned. Over all slices, the angle θ equals 45° with a deviation of $\pm 0.5°$ corresponding to the precision of the trace determination. Notice the good agreement with the calculated $\theta_{\{111\}}$ (see Fig. 6). Moreover, no deterioration of the focus was observed neither on the SEM images nor on the EBSD pattern quality images. All these results indicate that the beam shift and beam focus correction calculated from the theoretical slice thickness are sufficient to track the region of interest in our static experimental set-up.
(3) A good alignment of the raw data was observed in z direction. This is confirmed by the fact that the targeted twin plane was found to be close to the theoretical {111} twin plane. The experimental elevation angle of the boundary normal was found equal to $\psi = 59.3°$ close to the elevation angle of the theoretical {111} plane $\psi_{\{111\}}$=60.6° (see Fig. 6).
(4) Finally, because stage movements are eliminated in the static setup, the speed of 3D EBSD acquisition in the FIB–SEM is increased. In a non-static setup the acquisition of each data slice involves two movements (see above). Two to three minutes can be easily spent for each stage movement, including stage settling time, and time spent on the image registration needed to reposition accurately FIB and SEM beams relative to the VOI. This translates in our experiment in a time saving of 2–3 min/slice $\times$ 2 $\times$ 75 slices = 5–7.5 h i.e. a throughput increase of 15–25%.

As an outlook, 3D EBSD analysis throughput could even be increased further by performing the EBSD measurement while milling. Of course, a prerequisite is to be able to index the EBSD patterns despite the noise introduced by FIB. To explore this possibility, EBSD patterns of a selected grain were measured while milling at different currents (the pattern acquisition parameters were exactly the same as those used in the 3D EBSD experiment). Fig. 9 summarizes the results. The EBSD patterns are of sufficient quality for accurate indexing even if they are acquired while simultaneously FIB polishing using a FIB current as high as 30 nA (see Fig. 9(c)). Although, this might not hold true for other materials, it is a route worth exploring further in the future.

5. Summary

An optimized setup for automatic 3D EBSD tomography in a conventional FIB–SEM system has been developed. This setup requires no stage/sample movements between the FIB milling and EBSD scans. It shows clear advantages in terms of data throughput and quality. A twinned grain in an INCONEL 718 sample was used as a model system to demonstrate and discuss the quality of the raw 3D EBSD data. In the experiment, the same EBSD angular resolution was obtained across the slices as within each slice. Moreover the twin plane reconstructed from the unprocessed data was found to be a coherent {111} plane within 1°. This demonstrates the good alignment of the raw data in z direction. This precision is not achievable using other 3D EBSD setups. Consequently the 3D EBSD static setup offers new insights in 3D grain boundary engineering research.

Furthermore, we have shown that the static method provides a throughput improvement of up to 25% as compared to the tilt and rotation methods. Moreover, preliminary experiments show that EBSD pattern collection during FIB milling is possible, opening up new opportunities to increase 3D EBSD throughput even further.

Acknowledgments

This work was supported by the French State through the program “Investment in the future” operated by the National Research Agency (ANR) (ANR-11-LABX-0008-01).

References

[1] F.J. Humphreys, Grain and subgrain characterization by electron backscatter diffraction, J. Mater. Sci. 36 (2001) 3833–3854.

[2] M. Uchic et al., An Automated Multi-Modal Serial Sectioning System for Characterization of Grain-Scale Microstructures in Engineering Materials, in: Proceedings of the 1st International Conference on 3D Materials Science, J. Wiley & Sons, 2012, pp. 195 202.

[3] M.P. Echlin, et al., Three-dimensional characterization of the permeability of W–Cu composites using a new "TriBeam" technique, Acta Mater. 64 (2014) 307–315.

[4] S. Zaefferer, S.I. Wright, Three-dimensional orientation microscopy by serial sectioning and ebsd-based orientation mapping in a FIB-SEM, Electron Backscatter Diffraction in Materials Science, Springer (2009), p. 109–122 (chapter8).

[5] M.A. Groeber, et al., 3D reconstruction and characterization of polycrystalline microstructures using a FIB–SEM system, Mater. Charact. 57 (2006) 259–273.

[6] S. Zaefferer, S.I. Wright, D. Raabe, 3D-orientation microscopy in a FIB SEM: a new dimension of microstructure characterization, Metall. Mater. Trans. 39A (2008) 374–389.

[7] X. Man, et al., Materials analysis using a new concept: real-time three-dimensional analytical FIB-SEM, Microsc. Anal. 15 (2014) 15–20.

[8] D. Dönitz, Ch. Wagner, US Patent US8901510 B2, 2014.

[9] (a) M.A. Groeber, M.A. Jackson, DREAM.3D: A Digital Representation Environment for the Analysis of Microstructure in 3D, Integr. Mater. Manuf. Innov. 3 (2014) 5; (b) A. Henderson et al., The ParaView Guide, Kitware Inc., NY (2004).